



Tropospheric warming over the northern Indian Ocean caused by South Asian anthropogenic aerosols: possible impact on the upper troposphere and lower stratosphere

Suvarna Fadnavis¹, Prashant Chavan¹, Akash Joshi², Sunil M. Sonbawne¹, Asutosh Acharya³, Panuganti C. S. Devara⁴, Alexandru Rap⁵, Felix Ploeger⁶, and Rolf Müller⁶

¹Indian Institute of Tropical Meteorology, Center for Climate Change Research, MoES, Pune, India

²Indian Institute of Technology, Kharagpur, India

³Indian Institute of Technology, Bhubneshwar, India

⁴Centre of Excellence in ACOAST/ACESH, Amity University Haryana (AUH), Gurugram 122413, India

⁵School of Earth and Environment, University of Leeds, Leeds, UK

⁶Forschungszentrum Jülich GmbH, IEK-7, Jülich, Germany

Correspondence: Suvarna Fadnavis (suvarna@tropmet.res.in)

Received: 22 November 2021 – Discussion started: 1 December 2021

Revised: 29 April 2022 – Accepted: 2 May 2022 – Published: 3 June 2022

Abstract. Atmospheric concentrations of South Asian anthropogenic aerosols and their transport play a key role in the regional hydrological cycle. Here, we use the ECHAM6-HAMMOZ chemistry–climate model to show the structure and implications of the transport pathways of these aerosols during spring (March–May). Our simulations indicate that large amounts of anthropogenic aerosols are transported from South Asia to the northern Indian Ocean and western Pacific. These aerosols are then lifted into the upper troposphere and lower stratosphere (UTLS) by the ascending branch of the Hadley circulation, where they enter the westerly jet. They are further transported to the Southern Hemisphere ($\sim 15\text{--}30^\circ\text{S}$) and downward (320–340 K) via westerly ducts over the tropical Atlantic ($5^\circ\text{S}\text{--}5^\circ\text{N}$, $10\text{--}40^\circ\text{W}$) and Pacific ($5^\circ\text{S}\text{--}5^\circ\text{N}$, $95\text{--}140^\circ\text{E}$). The carbonaceous aerosols are also transported to the Arctic, leading to local heating (0.08–0.3 K per month, an increase by 10%–60%).

The presence of anthropogenic aerosols causes a negative radiative forcing (RF) at the top of the atmosphere (TOA) ($-0.90 \pm 0.089\text{ W m}^{-2}$) and surface ($-5.87 \pm 0.31\text{ W m}^{-2}$) and atmospheric warming ($+4.96 \pm 0.24\text{ W m}^{-2}$) over South Asia ($60\text{--}90^\circ\text{E}$, $8\text{--}23^\circ\text{N}$), except over the Indo-Gangetic Plain ($75\text{--}83^\circ\text{E}$, $23\text{--}30^\circ\text{N}$), where RF at the TOA is positive ($+1.27 \pm 0.16\text{ W m}^{-2}$) due to large concentrations of absorbing aerosols. The carbonaceous aerosols lead to in-atmospheric heating along the aerosol column extending from the boundary layer to the upper troposphere (0.1 to 0.4 K per month, increase by 4%–60%) and in the lower stratosphere at $40\text{--}90^\circ\text{N}$ (0.02 to 0.3 K per month, increase by 10%–60%). The increase in tropospheric heating due to aerosols results in an increase in water vapor concentrations, which are then transported from the northern Indian Ocean–western Pacific to the UTLS over $45\text{--}45^\circ\text{N}$ (increasing water vapor by 1%–10%).

1 Introduction

Understanding the variability of anthropogenic aerosol loading over the northern Indian Ocean is of utmost importance since (1) it regulates the Asian hydrological cycle via modulating atmospheric convection, heating rates, and moisture transport (Ramanathan et al., 2005; Corrigan et al., 2008; Budhavant et al., 2018; Meehl et al., 2008) and (2) it leads to adverse impacts on marine ecosystems (Mahowald et al., 2018; Collins et al., 2019). Several observations indicate that the aerosol loading over the northern Indian Ocean during the spring season is strongly influenced by South Asian aerosols. Aircraft measurements during the Indian Ocean Experiment (INDOEX) (February–March 1999) showed the presence of a thick layer (surface to 3.2 km) of anthropogenic aerosols (black carbon (BC) $\sim 14\%$, sulfate 34%, ammonium 11%) over the northern Indian Ocean (Dickerson et al., 2002; Mayol-Bracero et al., 2002) with sources over South Asia. Several other in situ observations, e.g., over the Maldives during November 2014–March 2015, show that air masses arising from the Indo-Gangetic Plain contain very high amounts (97%) of elemental carbon in the PM₁₀ in the fine mode. (Bhuhvant et al., 2018). Observations from the Geosphere-Biosphere Programme over the Bay of Bengal during spring (March 2016) also show abundant anthropogenic aerosols (sulfate and nitrate) having sources over the Indo-Gangetic Plain (Nair et al., 2017).

The aerosol loading over South Asia has been increasing at an alarming rate (rate of increase in aerosol optical depth (AOD) 0.004 yr^{-1} during 1988–2013) (Babu et al., 2013). For the last 2 decades, the AOD increase (by 12%) over South Asia has been attributed to the strong increase in anthropogenic aerosols (sulfate, black carbon, and organic carbon), while natural aerosol remained unchanged (Ramachandran et al., 2020a). The major sources of anthropogenic aerosols are the combustion of domestic fuels, industrial emissions, transportation, and open burning (Paliwal et al., 2016). The growth of the economy of India led to a 41% increase in BC and 35% in organic carbon (OC) from 2000 to 2010 (Lu et al., 2011). The emissions of sulfur dioxide (SO₂) which leads to the production of sulfate aerosols have doubled during 2006–2017 (Fadnavis et al., 2019). Figure 1a–c show the annual mean emission of BC, OC, and sulfate aerosols over South Asia in 2016 from the AEROCOM-ACCMIP-II emission inventory (discussed in Sect. 2.1). It shows high emissions over the Indo-Gangetic Plain (BC 7×10^{-12} – $17 \times 10^{-12} \text{ kg m}^{-2} \text{ s}^{-1}$, OC: 25×10^{-12} – $70 \times 10^{-12} \text{ kg m}^{-2} \text{ s}^{-1}$, sulfate: 2×10^{-12} – $5 \times 10^{-12} \text{ kg m}^{-2} \text{ s}^{-1}$). Higher amounts of aerosols over the Indo-Gangetic Plain are associated with densely populated regions and industrial and vehicular emissions (Karambelas et al., 2018; Fadnavis et al., 2019). Past studies also show substantially higher amounts of aerosols over northern India compared to the rest of the Indian region (Ramachandran et al., 2020b; Fadnavis et al., 2013, 2017a, b). Over the

Indo-Gangetic Plain, these emissions show a peak in spring (Fig. 1d), with increases for BC of 0%–3%, OC of 0%–8.7%, and sulfate of 0%–0.2%, compared to annual means. This peak in emissions in spring is to a large extent driven by springtime agricultural crop burning and biomass burning activity (Chavan et al., 2021).

While the presence of sulfate aerosols leads to a cooling of the atmosphere below due to their strong scattering properties, carbonaceous aerosols produce atmospheric warming via absorption of solar radiation (Fadnavis et al., 2019; Penner et al., 1998). Previous studies showed that the doubling of carbonaceous aerosols loading over South Asia (10° S–50° N, 65–155° E) led to significant atmospheric warming (in-atmospheric radiative forcing (RF) 5.11 W m^{-2} ; Fadnavis et al., 2017b).

During spring, the prevailing convective instability over the Bay of Bengal and the Arabian Sea transports aerosol from the boundary layer to the upper troposphere (Romatschke and Houze, 2011). Airborne observations during winter and spring, e.g., the Civil Aircraft for Regular Investigation of the Atmosphere based on an Instrument Container (CARIBIC) in March 1999 and January 2001 (Papaspiropoulos et al., 2002) and the Indian Ocean Experiment (INDOEX) in February–March 1999, show elevated aerosol amounts near 8–12 km over the Indian Ocean and South Asia (De Reus et al., 2001). Recently, using a set of model simulations, Chavan et al. (2021) reported the transport of biomass burning aerosols to the upper troposphere by convection in spring 2013.

Here, we investigate the source of the very large aerosol loading over the Arabian Sea during spring and their vertical transport to the upper troposphere and lower stratosphere (UTLS). We show these aerosols produce atmospheric warming, leading to enhanced water vapor that is transported to the UTLS. Once in the lower stratosphere, aerosols and water vapor are transported to the Southern Hemisphere ($\sim 45^\circ \text{ S}$), with implications for tropospheric temperatures and stratospheric ozone concentrations. For this purpose, we performed a series of five simulations using the ECHAM6-HAMMOZ model in order to investigate the impact of changes in anthropogenic aerosol over South Asia. The paper is structured as follows: the ECHAM6-HAMMOZ model simulations are provided in Sect. 2, and in Sect. 3 we discuss the results on the transport of South Asian aerosols to the northern Indian Ocean, radiative forcing, transport into the UTLS, and associated impacts on heating rates, while conclusions are summarized in Sect. 4.

2 Model simulations

2.1 ECHAM6-HAMMOZ experimental setup

We use the state-of-the-art chemistry–climate model ECHAM6-HAMMOZ. It comprises the general circulation module ECHAM6, coupled to the aerosol and cloud micro-

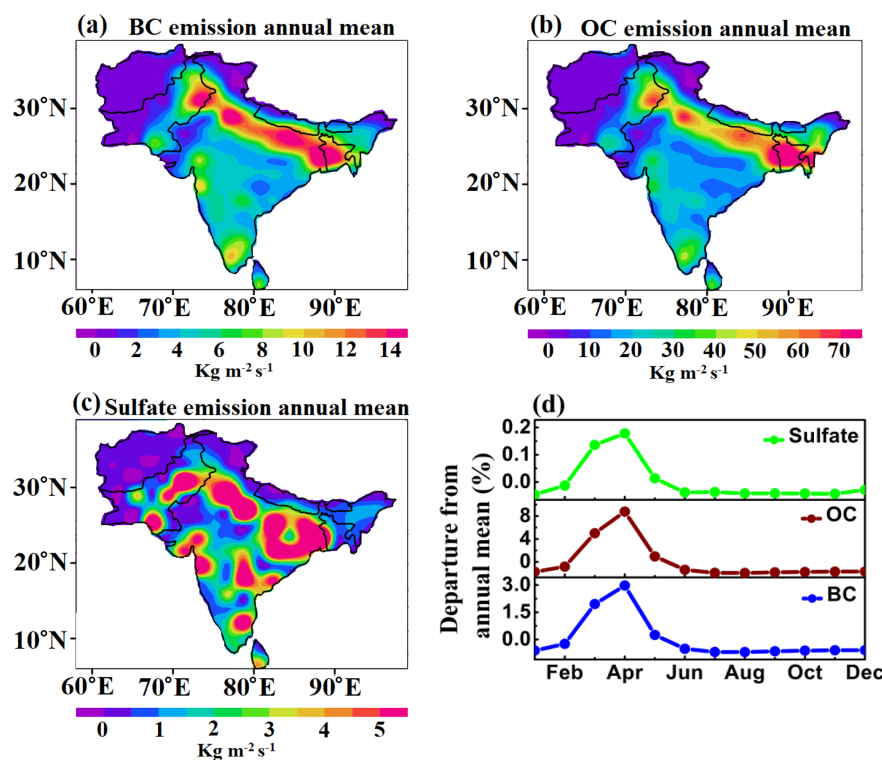


Figure 1. Spatial distribution for the year 2016 annual mean total emission ($\text{kg m}^{-2} \text{s}^{-1}$) of (a) BC, (b) OC, and (c) sulfate aerosols from the AEROCOM-ACCMIP-II emission inventory and (d) time series of monthly departure from annual mean total emissions (%) of BC, OC, and sulfate aerosols averaged over the Indo-Gangetic Plain ($23\text{--}30^\circ \text{N}$, $78\text{--}90^\circ \text{E}$).

physics module Hamburg (HAM) (Stier et al., 2005; Tegen et al., 2019). HAM predicts the nucleation, growth, evolution, and sinks of sulfate, black carbon (BC), organic carbon (OC), sea salt (SS), and mineral dust (DU) aerosols. The size distribution of the aerosol population is described by seven log-normal modes (nucleation mode, soluble and insoluble Aitken, soluble and insoluble accumulation, and soluble and insoluble coarse modes) (Stier et al., 2005; Zhang et al., 2012; Tegen et al., 2019). Moreover, HAM explicitly simulates the impact of aerosol species on cloud droplet and ice crystal formation according to prescribed microphysical properties. Aerosol particles can act as cloud condensation nuclei or as kernels for ice-nucleating particles. Other relevant cloud microphysical processes such as evaporation of cloud droplets, sublimation of ice crystals, ice crystal sedimentation, and detrainment of ice crystals from convective cloud tops are simulated interactively (Neubauer et al., 2014). The anthropogenic and fire emissions of sulfate, black carbon (BC), and organic carbon (OC) are based on the AEROCOM-ACCMIP-II emission inventory. Other details of the model and emissions are reported by Fadnavis et al. (2017a, 2019, 2021a, b).

The model simulations are performed at a T63 spectral resolution, corresponding to $1.875^\circ \times 1.875^\circ$ in the horizontal dimension, while the vertical resolution is described by 47

hybrid σ - p levels from the surface up to 0.01 hPa (approx. 80 km). The simulations have been carried out with a time step of 20 min. Monthly varying Atmospheric Model Intercomparison Project (AMIP) sea surface temperature (SST) and sea ice cover (SIC) (Taylor et al., 2000) were used as lower boundary conditions.

We performed five model experiments: (1) a control (CTL) simulation where all aerosol emissions are included and four perturbed experiments where (2) all anthropogenic aerosol emissions (black carbon, organic carbon, and sulfate) are switched off over South Asia ($75\text{--}100^\circ \text{E}$, $8\text{--}40^\circ \text{N}$; see Fig. 1) during the study period (2001–2016) (referred to as Aerooff), (3) only anthropogenic black carbon emissions (BC) are switched off during the study period (BCoff), (4) only anthropogenic organic carbon (OC) emissions are switched off (OCoff) during the study period, and (5) only anthropogenic sulfate aerosol emissions are switched off (Suloff) during the study period (see Table 1). All simulations were performed from 1 January 2001 to December 2016 from stabilized initial fields created after a model integration for 1 year. Dust emission parameterization is the same in all the simulations and is based on Tegen et al. (2002). The analysis is performed for spring (March–May) averaged for the period 2001–2016. We compare the CTL with Aerooff, BCoff, OCoff, and Suloff simulations to

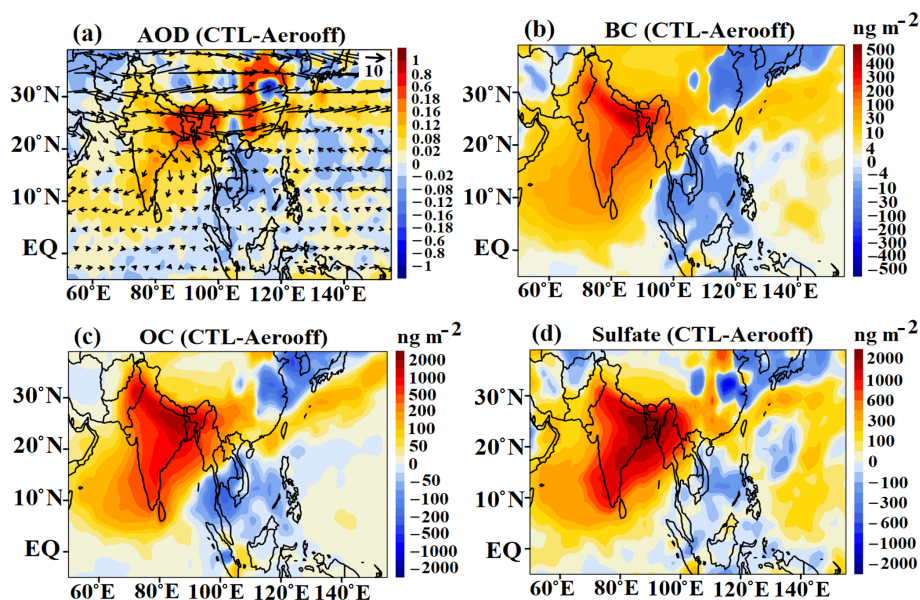


Figure 2. Spatial distribution of (a) AOD anomalies averaged for spring during 2001–2016 (CTL-Aerooff) and anomalies of tropospheric column of (b) BC, (c) OC, and (d) sulfate aerosols (ng m^{-2}) (CTL-Aerooff). The vectors in Fig. 2a indicate winds (m s^{-1}) at 850 hPa.

understand (1) transport pathways of South Asian anthropogenic aerosols and (2) their impact over the Indian region and UTLS (340–400 K). We compare AOD from CTL simulations with MISR and MODIS data (Sect. S1 in the Supplement). The model performance against MISR and MODIS (Kahn et al., 2007) for the spring season is discussed in Sect. S2 and Fig. S1 in the Supplement. We use the 2 PV contour in midlatitudes and the 380 K isentrope in the tropics as an estimate of the location of the dynamical tropopause (Holton et al., 1995). Note that the PV value at the dynamical tropopause is often somewhat higher than 2 PV and exhibits a certain variability (Kunz et al., 2011).

3 Results and discussions

3.1 Transport of South Asian aerosols to the northern Indian Ocean

The spatial distribution of AOD anomalies from the CTL-Aerooff simulation shows positive anomalies of AOD extending from South Asia to the Arabian Sea and the northern Bay of Bengal (10–20° N) (Fig. 2a). The wind vectors indicate that these are transported from the Indo-Gangetic Plain to the Arabian Sea, the Bay of Bengal, and the western Pacific. The transported aerosols enhanced the AOD by 0.18 %–0.8 % (30 %–80 %) over the northern Bay of Bengal and by 0.02 %–0.12 % (20 %–60 %) over the Arabian Sea. This is consistent with previous studies where 50 %–60 % enhancements in the AOD over the tropical Indian Ocean due to anthropogenic aerosols have been reported (Satheesh et al., 2000; Jose et al., 2020). Chemical analysis of aerosols observed over the southeastern coastal Arabian Sea also shows

the dominance of anthropogenic aerosols having sources over the Indian region (73 %) (Aswini et al., 2020). Analysis of MODIS satellite observations (2003–2017) likewise shows that anthropogenic sources contributed $\sim 60\%$ – 70% to the aerosol loading over the east coast and west coast of India (Jose et al., 2020).

The distribution of anomalies of the tropospheric column of BC, OC, and sulfate aerosols also indicates that these aerosols are transported from South Asia to the Bay of Bengal and the Arabian Sea (Fig. 2b–d). Enhancement of sulfate and OC aerosol ($50\text{--}2000 \text{ ng m}^{-2}$) is higher than BC ($4\text{--}500 \text{ ng m}^{-2}$) over the South Asian region (Fig. 2b–d). The total carbonaceous aerosol (BC and OC together) dominates over the sulfate aerosols. These anthropogenic aerosols over the tropical Indian Ocean affect the radiation budget and cloud cover over the Indian Ocean (Satheesh et al., 2000; McFarquhar and Wang, 2006).

3.2 Radiative forcing

Anthropogenic aerosols over the tropical Indian Ocean affect the radiation budget and cloud cover (McFarquhar and Wang, 2006). Here, we discuss the impact of South Asian anthropogenic aerosols on RF. Figure 3a–c show anomalies in net RF at the top of the atmosphere (TOA), surface, and in-atmosphere (TOA–surface) for Aerooff simulations (CTL-Aerooff). The anthropogenic aerosols have produced a cooling at the TOA (except over the Indo-Gangetic Plain) and at the surface (see Fig. 3a–b). The simulated RF values over the Arabian Sea ($55\text{--}70^\circ \text{ E}$, $8\text{--}20^\circ \text{ N}$), Bay of Bengal ($88\text{--}92^\circ \text{ E}$, $12\text{--}20^\circ \text{ N}$), and Indo-Gangetic Plain ($75\text{--}83^\circ \text{ E}$, $26\text{--}30^\circ \text{ N}$) are tabulated in Table S1 in the Supple-

Table 1. Details of ECHAM6-HAMMOZ model simulations performed in this study.

Experiment name	Duration	Aerosol species on/off	Boundary conditions
CTL	2001–2016	All aerosols species globally, as per AEROCOM-ACCMIIP-II emission inventory.	AMIP sea surface temperature and sea ice concentration.
Aerooff	2001–2016	Anthropogenic BC, OC, and sulfate aerosols switch off over South Asia during 2001–2016.	AMIP sea surface temperature and sea ice concentration.
BCoff	2001–2016	Anthropogenic BC aerosols switch off over South Asia during 2001–2016.	AMIP sea surface temperature and sea ice concentration.
OCoff	2001–2016	Anthropogenic OC aerosols switch off over South Asia during 2001–2016.	AMIP sea surface temperature and sea ice concentration.
Suloff	2001–2016	Anthropogenic sulfate aerosols switch off over South Asia during 2001–2016.	AMIP sea surface temperature and sea ice concentration.

ment. The RF estimates show that the aerosols have produced cooling at the TOA and surface over the Arabian Sea (TOA: $-0.72 \pm 0.14 \text{ W m}^{-2}$, surface: $-3.0 \pm 0.28 \text{ W m}^{-2}$), Bay of Bengal (TOA: $-1.24 \pm 0.15 \text{ W m}^{-2}$, surface: $-5.14 \pm 0.44 \text{ W m}^{-2}$), and in-atmospheric warming over the above regions (Arabian Sea $+2.27 \pm 0.19 \text{ W m}^{-2}$; Bay of Bengal: $+3.89 \pm 0.30 \text{ W m}^{-2}$) (Fig. 3c). The Indo-Gangetic Plain shows positive anomalies of RF at the TOA ($+1.27 \pm 0.16 \text{ W m}^{-2}$), negative at the surface ($-11.16 \pm 0.50 \text{ W m}^{-2}$), and an atmospheric warming of $+12.44 \pm 0.42 \text{ W m}^{-2}$. In agreement with our results, previous studies have reported negative RF at the surface and TOA and atmospheric warming over the northern Indian Ocean caused by enhanced anthropogenic aerosol. For example, Pathak et al. (2020) reported negative aerosol RF at the TOA (-2 to -4 W m^{-2}) over the Bay of Bengal and the Arabian Sea during spring 2009–2013. The clear-sky aerosol direct radiative forcing estimated from measurements during the INDOEX experiment (January to March in 1999) over the northern Indian Ocean also show similar results (TOA: -7 W m^{-2} , surface: -23 W m^{-2} , and in-atmosphere: $+16 \text{ W m}^{-2}$) (Ramanathan et al., 2001). There is a large variation in the magnitude of RF (at the TOA, surface, and in-atmosphere) reported from observations and our model simulations. This may be due to different regions and different time periods and the relatively coarse model resolution. The observation-based studies attribute positive in-atmospheric radiative forcing to absorbing aerosols (especially black carbon) that lead to a heating of the atmosphere (Rajeev and Ramanathan, 2001; Satheesh et al., 2002).

The analysis of the perturbed model experiments indicates that anthropogenic BC aerosols (Fig. 3d–f) have produced a warming at the TOA (Arabian Sea: $1.24 \pm 0.13 \text{ W m}^{-2}$, Bay of Bengal: $1.54 \pm 0.26 \text{ W m}^{-2}$, Indo-Gangetic Plain: $4.33 \pm 0.17 \text{ W m}^{-2}$) and cooling at the surface (Arabian Sea: $-2.56 \pm 0.25 \text{ W m}^{-2}$, Bay of Bengal: $-3.70 \pm 0.49 \text{ W m}^{-2}$, Indo-Gangetic Plain: $-9.27 \pm 0.37 \text{ W m}^{-2}$). OC (Fig. 3g–i) and sulfate (Fig. 3j–

l) aerosols have produced significant cooling at the TOA (OC: -0.21 ± 0.13 to $-0.44 \pm 0.15 \text{ W m}^{-2}$; sulfate: -1.55 ± 0.16 to $-2.14 \pm 0.17 \text{ W m}^{-2}$) and surface (OC: -0.49 ± 0.31 to $-2.56 \pm 0.45 \text{ W m}^{-2}$, sulfate: -1.19 ± 0.24 to $-2.67 \pm 0.36 \text{ W m}^{-2}$) over the above regions (listed in Table S1). Figure 3d, g, and j further confirm our finding that the positive anomalies of radiative forcing in the Indo-Gangetic Plain are due to BC aerosols because of their absorbing property. All the aerosols produce in-atmospheric warming over the Indian region (Fig. 3c, f, i, l) and the northern Indian Ocean (Fig. 3c, f, i). The atmospheric warming over the Arabian Sea and Bay of Bengal is due to BC and OC aerosols with larger contributions by the BC aerosols.

3.3 Transport of Asian anthropogenic aerosols into the UTLS

Further, we investigate the vertical distribution of aerosols that are transported to the northern Indian Ocean. This analysis is performed on isentropic levels, since past studies show that air mass transport from the troposphere to the stratosphere occurs largely along quasi-isentropic surfaces (Ploeger et al., 2017; Yan et al., 2021). In spring, Asian aerosols are transported partly to the Arabian Sea and Bay of Bengal region and partly to the western Pacific (Fig. 2a–d). Hence the meridional section is shown over the Indian Ocean and western Pacific region (30 – 140° E) (Fig. 4a–c). The vertical distribution of BC, OC, and sulfate aerosols indicates that these aerosols are transported from the boundary layer (10 – 30° N) into the UTLS (340 – 400 K) (Figs. 4a–c and S2). In the UTLS, at ~ 350 – 390 K they are transported southward ($\sim 30^\circ \text{ S}$) and downward (~ 320 – 340 K). The quasi-isentropic transport occurs via two pathways: (1) over Africa (20 – 60° E) and (2) over the East Indian Ocean and western Pacific (95 – 140° E) (Fig. 4d–f). The downward penetration of aerosols (BC, OC, and sulfate) in the Southern Hemisphere (15 – 30° S) to 320 – 340 K via the above-mentioned two pathways is also evident in Fig. 4g–i.

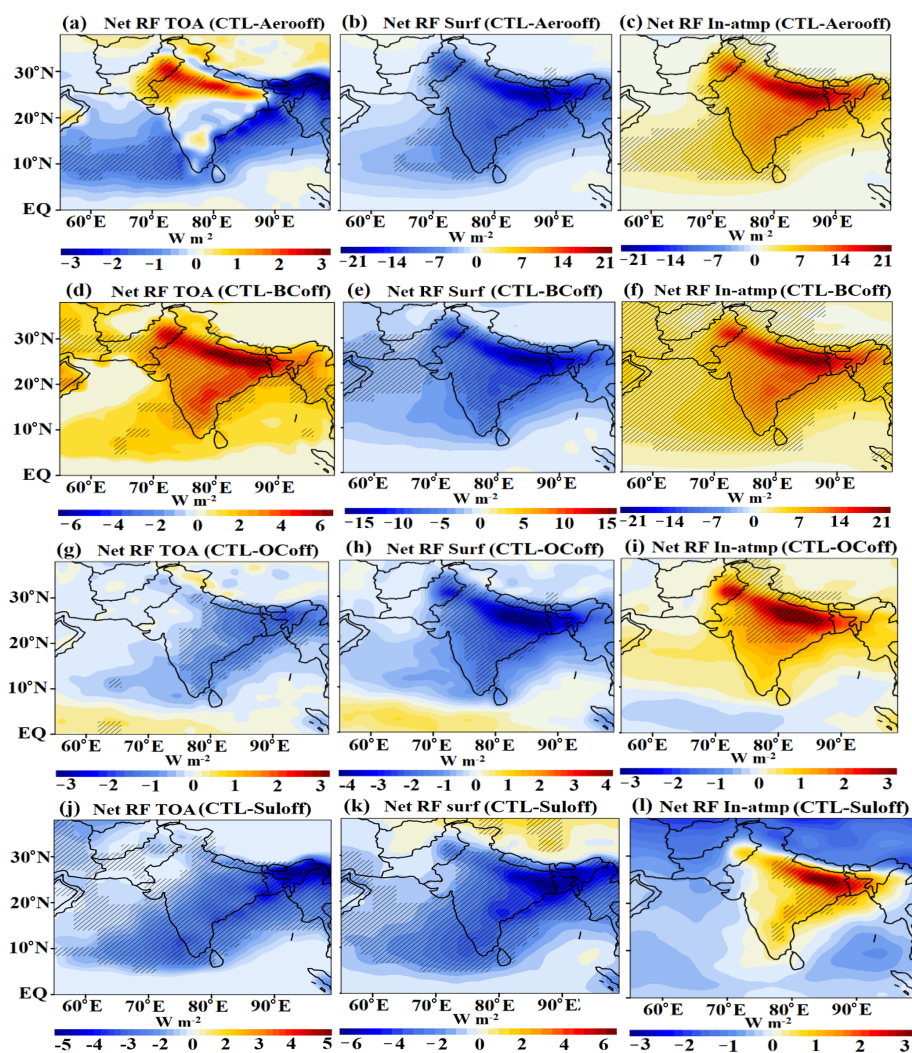


Figure 3. Spatial distribution of net aerosol radiative forcing (CTL-Aerooff) (W m^{-2}) averaged for spring for the years 2001–2016 for (a) TOA. (b) Same as (a) but for surface. (c) Same as (a) but for in-atmosphere (TOA–surface). (d) Spatial distribution of radiative forcing at the TOA (CTL-BCoff) averaged for spring for the years 2001–2016. (e) Same as (d) but for surface. (f) Same as (d) but for in-atmosphere (TOA–surface). (g) Spatial distribution of radiative forcing at the TOA (CTL-OCoff) averaged for spring during 2001–2016. (h) Same as (g) but for surface. (i) Same as (h) but for in-atmosphere (TOA–surface). (j) Spatial distribution of radiative forcing at the TOA (CTL-Suloff) averaged for spring during 2001–2016. (k) Same as (j) but for surface. (l) Same as (k) but for in-atmosphere (TOA–surface). The hatched lines in (a–l) indicate 99 % confidence level for the mean differences.

In the following, we further explore processes responsible for interhemispheric transport. Our analysis indicates that the Hadley circulation (Figs. 5a and S3) with its ascending branch over the Indian Ocean and adjoining region ($60\text{--}140^\circ\text{E}$, $0\text{--}30^\circ\text{N}$) lifts the South Asian aerosols to the UTLS. These aerosols enter the westerly jet (Fig. 4d–f).

The distribution of zonal winds in Fig. 5b shows transport into the Southern Hemisphere preferentially in regions of equatorial westerly winds, so-called “westerly duct” regions (Waugh and Polvani, 2000; Yan et al., 2021), where Rossby wave breaking occurs (Figs. 5b and S4). This is consistent with findings from Frederiksen et al. (2018), who have also shown interhemispheric transport of CO_2 via Pacific and

Atlantic westerly ducts during the spring season. Figure 5c shows that changes in South Asian aerosols concentrations cause a shift in the Pacific duct. Thus interhemispheric transport occurs through (1) an Atlantic duct and (2) a slightly shifted Pacific duct ($5^\circ\text{S}\text{--}5^\circ\text{N}$, $50\text{--}140^\circ\text{E}$), i.e. over the Indian Ocean–western Pacific region (also see Fig. 4d–f). The shift in Pacific duct as a response to South Asian aerosol changes is likely due to higher Rossby wave breaking near South Asia. The geopotential (Fig. 5d) and potential vorticity (Fig. S5) anomalies (CTL-Aerooff) show Rossby wave breaking near the Indian Ocean–western Pacific region that could lead to southern hemispheric transport through the Indian Ocean–western Pacific region path (Fig. 5c–d). In addi-

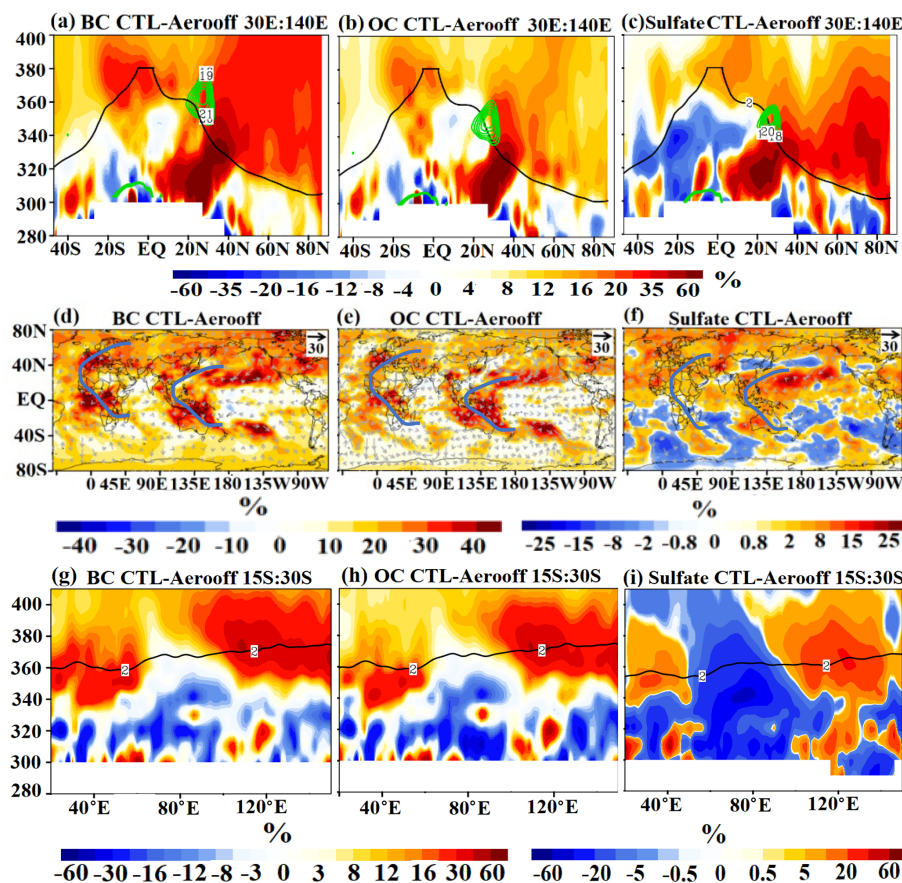


Figure 4. Meridional cross-section over Indian Ocean–western Pacific (averaged 30–140° E and for the spring season for the years 2001–2016) of anomalies (%) (CTL-Aerooff) of (a–c) BC, OC, and sulfate aerosols. Green contours in (a–c) indicate westerly jet. (d–f) Spatial distribution of BC, OC, and sulfate aerosols averaged at 360–390 K isentropic levels and the spring season for the years 2001–2016. Vectors in (d–f) indicate anomalies of winds (m s^{-1}). (g–i) Zonal cross-section (averaged over 15–30° S and for the spring season for the years 2001–2016) and for the spring season for BC, OC, and sulfate aerosols. The black line of 2 PV (in a–c and g–i) indicates the dynamical tropopause.

tion, the interhemispheric transport is also likely influenced by the monthly migration and the strength of the Hadley circulation (Fig. S3).

Further, in the UTLS, South Asian aerosols are transported to the Arctic (Fig. 4a–c). There is an aerosol enhancement in the Arctic (BC: 10% to 30%, OC: 10% to 20%, sulfate: 5% to 30%). Our analysis shows that transport to the Arctic occurs every year in the UTLS, which causes heating in the lower stratosphere (380–400 K) (see Sect. 3.4).

3.4 Impacts on the net heating rate and water vapor

Carbonaceous aerosols absorb solar radiation, leading to atmospheric heating, while predominately scattering aerosols such as sulfate reflect and scatter back solar radiation, therefore cooling the atmosphere below (Fadnavis et al., 2019). Here, we analyze net heating rates (shortwave + longwave) induced by all the anthropogenic Asian aerosols (CTL-Aerooff). Changes in the net heating rates are induced by

the aerosol changes; any changes in dynamical heating will be intrinsic. The vertical distribution of net heating rate anomalies over the northern Indian Ocean and western Pacific region (30–140° E) indicates increase in heating rates in the region of elevated anthropogenic aerosols in the troposphere (0.15 to 0.4 K per month, 5%–60%) and UTLS (0.02 to 0.3 K per month, 10%–60%) (Figs. 6a–d, 4, and S2). Heating rate anomalies estimated over the northern Indian Ocean and western Pacific region from BC (CTL-BCoff), OC (CTL-OCoff), and sulfate (CTL-Suloff) show that BC and OC aerosols produce heating in the troposphere (280–340 K) (10–40° N) (BC: 0.6 to 2 K per month, 10%–50%, OC: 0.2 to 0.4 K per month, 0.5%–4%) and UTLS over the Northern Hemisphere (BC: 0.08 to 0.2 K per month, 30%–45%, OC: 0.02 to 0.06 K per month, 0.2%–1.5%), while sulfate aerosols produce atmospheric cooling in the troposphere and UTLS of -0.02 to -0.4 K per month (5%–40%) (280–400 K) (Fig. 6a–d). Black carbon aerosol produces higher heating than organic carbon aerosols. The shortwave heating

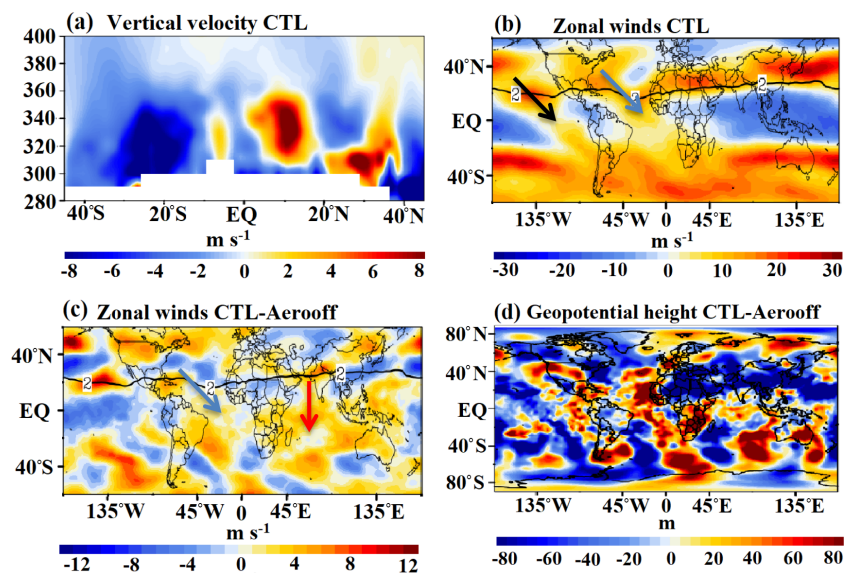


Figure 5. (a) Meridional cross-section of vertical velocities (m s^{-1}) (averaged for $65\text{--}140^\circ\text{E}$ and for spring season during 2001–2016). Vertical velocities are scaled by 300. (b) Zonal winds at the 360 K isentropic level from CTL simulations, where a black arrow indicates the Pacific duct, and a blue arrow indicates the Atlantic duct. (c) Anomalies (CTL-Aerooff) of zonal winds at the 360 K isentropic level. A blue arrow indicates the Atlantic duct, and a red arrow indicates the duct over the Indian Ocean. (d) Anomalies (CTL-Aerooff) of geopotential height (m) at the 340 K potential temperature level. The potential vorticity (2 PV) is indicated by the black contour in **b–c**.

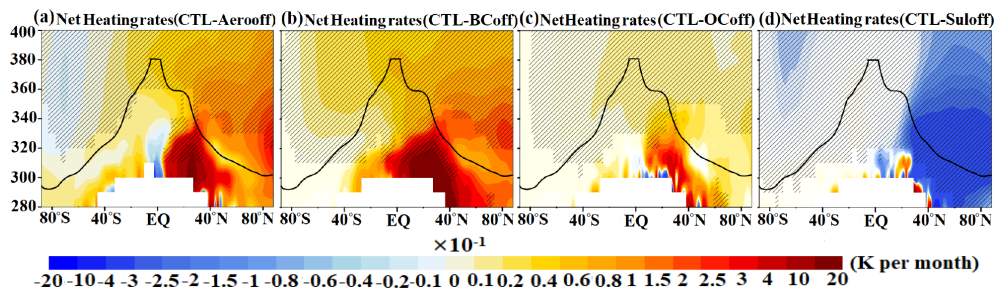


Figure 6. Meridional cross-section of heating rates (K per month) over the Indian Ocean–western Pacific (averaged $30\text{--}140^\circ\text{E}$ and for the spring season for the years 2001–2016) (a) from the CTL-Aerooff simulation. (b) Same (a) but from the CTL-BCoff simulation. (c) Same (a) but from the CTL-OCoff simulation. (d) Same (a) but from the CTL-Suloff simulation. Hatched lines in (a–d) indicate the 95 % significance level. A black line in (a–d) indicates the dynamical tropopause.

due to BC aerosols is the major contributor to the total heating. In general, these aerosols increase heating in the troposphere extending to the lower stratosphere (400 K) over the South Asian region (Fig. 6a). There is enhancement in heating rates along the path of aerosols transported to the Arctic.

The vertical distribution of water vapor over the Indian Ocean–western Pacific region ($30\text{--}140^\circ\text{E}$) (CTL-Aerooff) shows that water vapor concentrations are enhanced by 1 %–10 % along the path of elevated aerosols (Figs. 7a and 4). In the UTLS, water vapor is transported to the Southern Hemisphere $\sim 45^\circ\text{S}$. This may be due to heating caused by the Asian aerosols. The impact of BC (CTL-BCoff), OC (CTL-OCoff), and sulfate (CTL-Suloff) on the water vapor distribution (Fig. 7b–d) shows that BC aerosols play a major role in water vapor enhancement in the UTLS (Fig. 7b). Water

vapor enhancement by BC aerosols over the Indian Ocean–western Pacific region is $\sim 1\%$ – 15% (Fig. 7b). The water vapor enhancement by OC aerosols in the UTLS region is 0.8% – 15% (Fig. 7c) and by sulfate aerosols $\sim 0.2\%$ – 1% in pockets (Fig. 7d).

Although the focus of the paper is on the transport of aerosols during the spring season, it should be noted that anthropogenic South Asian aerosols are also transported to the UTLS during the monsoon season (Shindell et al., 2008; Fadnavis et al., 2013, 2017, 2019; Zheng et al., 2021). Annual distribution anomalies of aerosols (average of BC, OC, and sulfate) show the transport of aerosols into the UTLS during the spring and monsoon season (April to September) from the South Asian region (Fig. 8a). In the lower stratosphere, these aerosols persist for a few months (Fig. 8a);

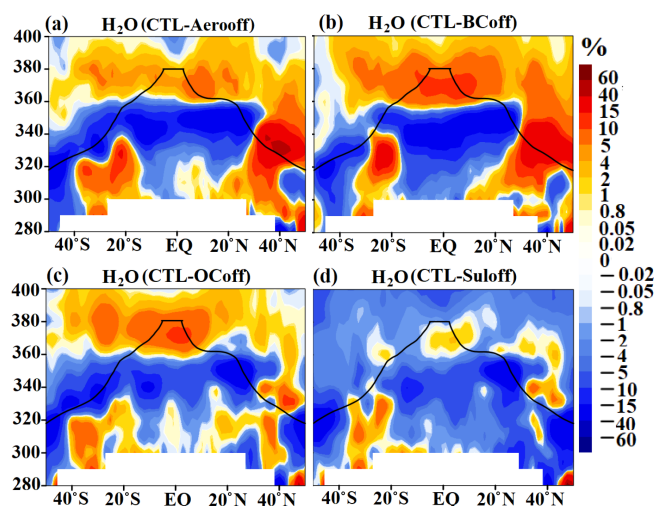


Figure 7. (a) Meridional cross-section over the Indian Ocean–western Pacific (averaged over 30–140° E) of anomalies of water vapor (%) (CTL-Aerooff) for the spring season for the years 2001–2016. (b) Same as (a) but from CTL-BCoff simulations. (c) Same as (a) but from CTL-OCoff simulations. (d) Same as (a) but from CTL-Suloff simulations. A black line in (a–d) indicates the dynamical tropopause.

thus their effect will be seen for an extended time. These aerosols enhance tropospheric heating, thereby transporting elevated water vapor into the lower stratosphere (Fig. 8b). Figure 8a also shows the transport of aerosols into the lower stratosphere during spring and the monsoon seasons (March–September). The aerosol-induced enhanced water vapor also shows enhancement in the lower stratosphere during the same time (Fig. 8b).

Further, we analyze the correlation between heating rates and carbonaceous aerosol amounts in the UTLS (380 K level) in the Arctic during 2001–2016 (spring mean) (Fig. 9) from Aerooff, BCoff, and OCoff in comparison with CTL simulations. The carbonaceous aerosols show a positive correlation (correlation coefficient r : 0.55 to 0.85) with the UTLS heating rates, indicating that transported carbonaceous aerosols enhance UTLS heating in the Arctic. It should be noted that increase in aerosols at the Arctic also occurs during the monsoon season (Fadnavis et al., 2017a, b, 2019; Zheng et al., 2021), which may affect the dynamics and aerosol amounts in the spring of the next year in the UTLS.

Importantly, South Asian aerosols enhance water vapor in the lower stratosphere in the tropical and subtropical latitudes (45° S–45° N). Water vapor, being a greenhouse gas, further enhances the heating of the troposphere, leading to a positive feedback. The increase in water vapor in the stratosphere also warms the Earth’s surface (Shindell, 2001; Solomon et al., 2010). Solomon et al. (2010) estimated that an increase in stratospheric water vapor by 1 ppmv accounts for 0.24 W m⁻² radiative forcing at the TOA. The SABER and MLS observations showed an increase in stratospheric water

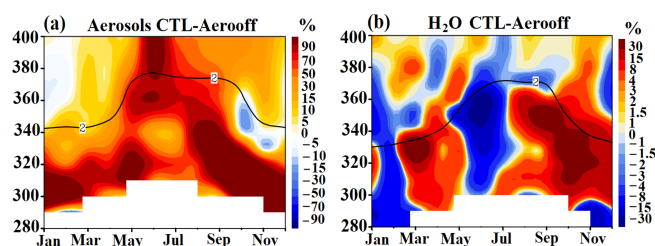


Figure 8. (a) Annual distribution of anomalies of aerosols (CTL-Aerooff) (averaged of BC, OC and sulfate aerosols) (%) averaged over the South Asian region (50–100° E, 20–40° N). (b) same as (a) but for water vapor (%) over the northern Indian Ocean–western Pacific (30–140° E, 20–40° N). A black line in (a–b) indicates the dynamical tropopause.

vapor by 0.45 ppmv globally during 2003–2017 (Yue et al., 2019). Thus the radiative forcing due to water vapor increase (0.02–0.14 ppmv) in response to South Asian anthropogenic aerosols is not negligible for surface warming globally. Further, increasing stratospheric water vapor could also lead to ozone depletion (e.g., Shindell, 2001; Robrecht et al., 2019).

4 Conclusions

A series of ECHAM6-HAMMOZ chemistry–climate simulations for South Asian anthropogenic aerosols were used to understand the transport pathways of South Asian aerosols in spring and their impacts on the UTLS. The model simulations show that large amounts of South Asian aerosols are transported during spring to the Arabian Sea (increases in AOD by 0.02–0.12 from CTL-Aerooff) and Bay of Bengal (increases in AOD by 0.16 to 0.8 from CTL-Aerooff) and western Pacific (increases in AOD by 0.08 to 0.18). These aerosols are further lifted up into the UTLS from the northern Indian Ocean and South Asia (10–30° N). In the UTLS, they are also transported to the Southern Hemisphere (15–30° S) and downward (320–340 K). The processes responsible for interhemispheric transport are as follows:

1. South Asian aerosols are lifted up to the UTLS by the ascending branch of the Hadley circulation. In the UTLS, the aerosols enter the westerly jet.
2. They are transported to the Southern Hemisphere via the Atlantic westerly duct (5° S–5° N, 10–40° W) and Pacific westerly duct (5° S–5° N, 50–140° E).
3. A shift in the Pacific westerly duct may be due to an increase in Rossby wave breaking over the northern Indian Ocean–western Pacific, induced by South Asian aerosols.

Anthropogenic aerosol produces significant radiative impacts over the Indo-Gangetic Plain (RF anomalies estimated from CTL-Aerooff simulations, TOA: $+1.27 \pm 0.16$ W m⁻²,

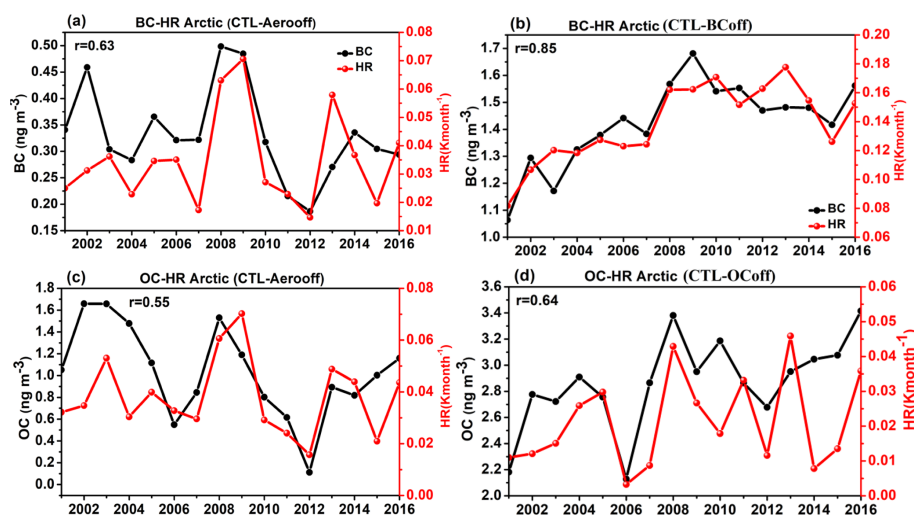


Figure 9. (a) Time series of BC aerosols and heating rates averaged for spring in the UTLS (380 K) in the Arctic ($65\text{--}85^\circ\text{N}$, $0\text{--}360^\circ$) (from CTL-Aerooff). (b) Same as (a) but from CTL-BCoff. (c) Same as (a) but for OC. (d) Same as (c) but from CTL-OCoff. The correlation coefficient (r) between anomalies of BC / OC aerosols and heating rates is indicated in (a–d).

surface: $-11.16 \pm 0.50 \text{ W m}^{-2}$, in-atmosphere: $+12.44 \pm 0.42 \text{ W m}^{-2}$) and the Arabian Sea (RF at the TOA: $-0.72 \pm 0.14 \text{ W m}^{-2}$, surface: $-3.00 \pm 0.28 \text{ W m}^{-2}$, in-atmosphere: $+2.27 \pm 0.19 \text{ W m}^{-2}$). Interestingly, RF at the TOA over the Indo-Gangetic Plain is positive ($+4.33 \pm 0.17 \text{ W m}^{-2}$) due to the emission of BC aerosols alone. Anthropogenic aerosols enhance heating in the troposphere over the northern Indian Ocean (estimated from CTL-Aerooff) by 0.15 to 0.4 K per month (4%–60%) and the UTLS by 0.02 to 0.3 K per month (10%–60%).

The heating of the troposphere by carbonaceous aerosol (mainly BC) increases temperature and thereby tropospheric water vapor amounts over the northern Indian Ocean and adjoining regions. The elevated water vapor is transported to the UTLS from the northern Indian Ocean–western Pacific region ($30\text{--}40^\circ\text{E}$, $20\text{--}40^\circ\text{N}$). In the UTLS it is transported to the Southern Hemisphere at $\sim 45^\circ\text{S}$. BC aerosols play a major role in water vapor enhancement in the lower stratosphere (increased water vapor by 0.8%–5%). As water vapor is a greenhouse gas, this enhancement of stratospheric water vapor could potentially amplify the warming of the troposphere and surface and cause a positive feedback (e.g., Shindell, 2001; Solomon et al., 2010).

Data availability. The data used in this study are generated from ECHAM6-HAMMOZ model simulations at the High-Performance Computing system at the Indian Institute of Tropical Meteorology, Pune, India. The AOD data from MODIS Terra used here can be downloaded from <https://ladsweb.modaps.eosdis.nasa.gov/archive/allData/61/MODATML2/> (last access: 1 November 2021, NASA, 2021a) and MISR from <https://mISR.jpl.nasa.gov/getData/accessData/> (last access: 1 November 2021, NASA, 2021b).

Supplement. The supplement related to this article is available online at: <https://doi.org/10.5194/acp-22-7179-2022-supplement>.

Author contributions. SF initiated the idea. AJ, SS, and AA performed model analysis. RM and AR contributed to analysis and study design. All authors contributed to the writing and discussions of the manuscript.

Competing interests. At least one of the (co-)authors is a member of the editorial board of *Atmospheric Chemistry and Physics*. The peer-review process was guided by an independent editor, and the authors also have no other competing interests to declare.

Disclaimer. Publisher's note: Copernicus Publications remains neutral with regard to jurisdictional claims in published maps and institutional affiliations.

Acknowledgements. The authors thank the staff of the High-Performance Computing (HPC) system at the Indian Institute of Tropical Meteorology, Pune, India. We thank the reviewers for their valuable suggestions. We thank Jonathon Wright for useful discussions and suggestions that improved the quality of the manuscript.

Review statement. This paper was edited by Yves Balkanski and reviewed by Jonathon Wright and one anonymous referee.

References

- Aswini, A. R., Hegde, P., Aryasree, S., Girach, I. A., and Nair, P. R.: Continental outflow of anthropogenic aerosols over Arabian Sea and Indian Ocean during wintertime: ICARB-2018 campaign, *Sci. Total Environ.*, 712, 135214, <https://doi.org/10.1016/j.scitotenv.2019.135214>, 2020.
- Babu, S. S., Manoj, M. R., Moorthy, K. K., Gogoi, M. M., Nair, V. S., Kompalli, S. K., Satheesh, S. K., Niranjan, K., Ramagopal, K., Bhuyan, P. K., and Singh, D.: Trends in aerosol optical depth over Indian region: Potential causes and impact indicators, *J. Geophys. Res.-Atmos.*, 118, 11794–11806, <https://doi.org/10.1002/2013JD020507>, 2013.
- Budhavant, K., Bikkina, S., Andersson, A., Asmi, E., Backman, J., Kesti, J., Zahid, H., Satheesh, S. K., and Gustafsson, Ö.: Anthropogenic fine aerosols dominate the wintertime regime over the northern Indian Ocean, *Tellus B*, 70, 1–15, <https://doi.org/10.1080/16000889.2018.1464871>, 2018.
- Chavan, P., Fadnavis, S., Chakraborty, T., Sioris, C. E., Griessbach, S., and Müller, R.: The outflow of Asian biomass burning carbonaceous aerosol into the upper troposphere and lower stratosphere in spring: radiative effects seen in a global model, *Atmos. Chem. Phys.*, 21, 14371–14384, <https://doi.org/10.5194/acp-21-14371-2021>, 2021.
- Corrigan, C. E., Roberts, G. C., Ramana, M. V., Kim, D., and Ramanathan, V.: Capturing vertical profiles of aerosols and black carbon over the Indian Ocean using autonomous unmanned aerial vehicles, *Atmos. Chem. Phys.*, 8, 737–747, <https://doi.org/10.5194/acp-8-737-2008>, 2008.
- Collins, M., Sutherland, M., Bouwer, L., Cheong, S.-M., Frölicher, T. L., Jacot Des Combes, H., Roxy, M. K., Losada, I., McInnes, K. L., Ratter, B., Rivera-Arriaga, E., Susanto, R. D., Swingedouw, D., and Tibig, L.: Extremes, Abrupt Changes and Managing Risk, in: IPCC Special Report on the Ocean and Cryosphere in a Changing Climate, edited by: Pörtner, H.-O., Roberts, D. C., Masson-Delmotte, V., Zhai, P., Tignor, M., Poloczanska, E., Mintenbeck, K., Alegría, A., Nicolai, M., Okem, A., Petzold, J., Rama, B., and Weyer, N. M., Cambridge University Press, Cambridge, UK and New York, NY, USA, 589–655, <https://doi.org/10.1017/9781009157964.008>, 2019.
- De Reus, M., Krejci, R., Williams, J., Fischer, H., Scheele, R., and Ström, J.: Vertical and horizontal distributions of the aerosol number concentration and size distribution over the northern Indian Ocean, *J. Geophys. Res.-Atmos.*, 106, 28629–28641, <https://doi.org/10.1029/2001JD900017>, 2001.
- Dickerson, R. R., Andreae, M. O., Campos, T., Mayol-Bracero, O. L., Neusuess, C., and Streets, D. G.: Analysis of black carbon and carbon monoxide observed over the Indian Ocean: Implications for emissions and photochemistry, *J. Geophys. Res.*, 107, 8017, [doi:10.1029/2001JD000501](https://doi.org/10.1029/2001JD000501), 2002.
- Fadnavis, S. and Chattopadhyay, R.: Linkages of subtropical stratospheric intraseasonal intrusions with Indian summer monsoon deficit rainfall, *J. Climate*, 30, 5083–5095, <https://doi.org/10.1175/JCLI-D-16-0463.1>, 2017.
- Fadnavis, S., Semeniuk, K., Pozzoli, L., Schultz, M. G., Ghude, S. D., Das, S., and Kakatkar, R.: Transport of aerosols into the UTLS and their impact on the Asian monsoon region as seen in a global model simulation, *Atmos. Chem. Phys.*, 13, 8771–8786, <https://doi.org/10.5194/acp-13-8771-2013>, 2013.
- Fadnavis, S., Roy, C., Sabin, T. P., Ayantika, D. C., and Ashok, K.: Potential modulations of pre-monsoon aerosols during El Niño: impact on Indian summer monsoon, *Clim. Dynam.*, 49, 2279–2290, <https://doi.org/10.1007/s00382-016-3451-6>, 2017a.
- Fadnavis, S., Kalita, G., Kumar, K. R., Gasparini, B., and Li, J.-L. F.: Potential impact of carbonaceous aerosol on the upper troposphere and lower stratosphere (UTLS) and precipitation during Asian summer monsoon in a global model simulation, *Atmos. Chem. Phys.*, 17, 11637–11654, <https://doi.org/10.5194/acp-17-11637-2017>, 2017b.
- Fadnavis, S., Müller, R., Kalita, G., Rowlinson, M., Rap, A., Li, J.-L. F., Gasparini, B., and Laakso, A.: The impact of recent changes in Asian anthropogenic emissions of SO₂ on sulfate loading in the upper troposphere and lower stratosphere and the associated radiative changes, *Atmos. Chem. Phys.*, 19, 9989–10008, <https://doi.org/10.5194/acp-19-9989-2019>, 2019.
- Fadnavis, S., Sabin, T. P., Rap, A., Müller, R., Kubin, A., and Heinold, B.: The impact of COVID-19 lockdown measures on the Indian summer monsoon, *Environ. Res. Lett.*, 16, 074054, <https://doi.org/10.1088/1748-9326/ac109c>, 2021a.
- Fadnavis, S., Müller, R., Chakraborty, T., Sabin, T. P., Laakso, A., Rap, A., Griessbach, S., Vernier, J.-P., and Tilmes, S.: The role of tropical volcanic eruptions in exacerbating Indian droughts, *Sci. Rep.*, 11, 2714, <https://doi.org/10.1038/s41598-021-81566-0>, 2021b.
- Frederiksen, J. S. and Francey, R. J.: Unprecedented strength of Hadley circulation in 2015–2016 impacts on CO₂ inter-hemispheric difference, *Atmos. Chem. Phys.*, 18, 14837–14850, <https://doi.org/10.5194/acp-18-14837-2018>, 2018.
- Holton, J. R., Haynes, P. H., McIntyre, M. E., Douglass, A. R., Rood, R. B., and Pfister, L.: Stratosphere-troposphere exchange, *Rev. Geophys.*, 33, 403–439, <https://doi.org/10.1029/95RG02097>, 1995.
- Jose, S., Nair, V. S., and Babu, S. S.: Anthropogenic emissions from South Asia reverses the aerosol indirect effect over the northern Indian Ocean, *Sci. Rep.*, 10, 18360, <https://doi.org/10.1038/s41598-020-74897-x>, 2020.
- Karambelas, A., Holloway, T., Kinney, P. L., Fiore, A. M., Defries, R., Kieseewetter, G., and Heyes, C.: Urban versus rural health impacts attributable to PM_{2.5} and O₃ in northern India, *Environ. Res. Lett.*, 13, 064010, <https://doi.org/10.1088/1748-9326/aac24d>, 2018.
- Kahn, R. A., Garay, M. J., Nelson, D. L., Yau, K. K., Bull, M. A., Gaitley, B. J., Martonchik, J. V., and Levy, R. C.: Satellite-derived aerosol optical depth over dark water from MISR and MODIS: Comparisons with AERONET and implications for climatological studies, *J. Geophys. Res.*, 112, D18205, <https://doi.org/10.1029/2006JD008175>, 2007.
- Kunz, A., Konopka, P., Müller, R., and Pan, L. L.: The dynamical tropopause based on isentropic potential vorticity gradients *J. Geophys. Res.*, 116, D01110, <https://doi.org/10.1029/2010JD014343>, 2011.
- Lu, Z., Zhang, Q., and Streets, D. G.: Sulfur dioxide and primary carbonaceous aerosol emissions in China and India, 1996–2010, *Atmos. Chem. Phys.*, 11, 9839–9864, <https://doi.org/10.5194/acp-11-9839-2011>, 2011.
- Mahowald, N. M., Hamilton, D. S., Mackey, K. R. M., Moore, J. K., Baker, A. R., Scanza, R. A., and Zhang, Y.: Aerosol trace metal

- leaching and impacts on marine microorganisms, *Nat. Commun.*, 9, 2614, <https://doi.org/10.1038/s41467-018-04970-7>, 2018.
- Mayol-Bracero, O. L., Gabriel, R., Andreae, M. O., Kirchstetter, T. W., Novakov, T., Ogren, J., Sheridan, P., and Streets, D. G.: Carbonaceous aerosols over the Indian Ocean during the Indian Ocean Experiment (INDOEX): Chemical characterization, optical properties, and probable sources, *J. Geophys. Res.-Atmos.*, 107, 8030, <https://doi.org/10.1029/2000JD000039>, 2002.
- McFarquhar, G. M. and Wang, H.: Effects of aerosols on trade wind cumuli over the Indian Ocean: Model simulations, *Q. J. R. Meteorol. Soc.*, 132, 821–843, <https://doi.org/10.1256/qj.04.179>, 2006.
- Meehl, G. A., Arblaster, J. M., and Collins, W. D.: Effects of black carbon aerosols on the Indian monsoon, *J. Climate*, 21, 2869–2882, <https://doi.org/10.1175/2007JCLI1777.1>, 2008.
- Nair, V. S., Babu, S. S., Manoj, M. R., Moorthy, K. K., and Chin, M.: Direct radiative effects of aerosols over South Asia from observations and modeling, *Clim. Dynam.*, 49, 1411–1428, <https://doi.org/10.1007/s00382-016-3384-0>, 2017.
- NASA: MODIS, [data set], <https://ladsweb.modaps.eosdis.nasa.gov/archive/allData/61/MODATML2/>, last access: 1 November 2021a.
- NASA: MISR, [data set], <https://mistr.jpl.nasa.gov/getData/accessData/>, last access: 1 November 2021b.
- Neubauer, D., Lohmann, U., Hoose, C., and Frontoso, M. G.: Impact of the representation of marine stratocumulus clouds on the anthropogenic aerosol effect, *Atmos. Chem. Phys.*, 14, 11997–12022, <https://doi.org/10.5194/acp-14-11997-2014>, 2014.
- Paliwal, U., Sharma, M., and Burkhart, J. F.: Monthly and spatially resolved black carbon emission inventory of India: uncertainty analysis, *Atmos. Chem. Phys.*, 16, 12457–12476, <https://doi.org/10.5194/acp-16-12457-2016>, 2016.
- Papaspriopoulos, G., Martinsson, B. G., Zahn, A., Brenninkmeijer, C. A. M., Hermann, M., Heintzenberg, J., Fischer, H., and Van Velthoven, P. F. J.: Aerosol elemental concentrations in the tropopause region from intercontinental flights with the Civil Aircraft for Regular Investigation of the Atmosphere Based on an Instrument Container (CARIBIC) platform, *J. Geophys. Res.-Atmos.*, 107, 4671, <https://doi.org/10.1029/2002JD002344>, 2002.
- Pathak, H. S., Satheesh, S. K., Moorthy, K. K., and Nanjundiah, R. S.: Assessment of regional aerosol radiative effects under the SWAAMI campaign – Part 2: Clear-sky direct short-wave radiative forcing using multi-year assimilated data over the Indian subcontinent, *Atmos. Chem. Phys.*, 20, 14237–14252, <https://doi.org/10.5194/acp-20-14237-2020>, 2020.
- Penner, J. E., Chuang, C. C., and Grant, K.: Climate forcing by carbonaceous and sulfate aerosols, *Clim. Dynam.*, 14, 839–851, <https://doi.org/10.1007/s003820050259>, 1998.
- Ploeger, F., Konopka, P., Walker, K., and Riese, M.: Quantifying pollution transport from the Asian monsoon anticyclone into the lower stratosphere, *Atmos. Chem. Phys.*, 17, 7055–7066, <https://doi.org/10.5194/acp-17-7055-2017>, 2017.
- Rajeev, K. and Ramanathan, V.: Direct observations of clear-sky aerosol radiative forcing from space during the Indian Ocean Experiment, *J. Geophys. Res.-Atmos.*, 106, 17221–17235, <https://doi.org/10.1029/2000JD900723>, 2001.
- Ramachandran, S., Rupakheti, M., and Lawrence, M. G.: Aerosol-induced atmospheric heating rate decreases over South and East Asia as a result of changing content and composition, *Sci. Rep.*, 10, 20091, <https://doi.org/10.1038/s41598-020-76936-z>, 2020a.
- Ramachandran, S., Rupakheti, M., and Lawrence, M. G.: Black carbon dominates the aerosol absorption over the Indo-Gangetic Plain and the Himalayan foothills, *Environ. Int.*, 142, 105814, <https://doi.org/10.1016/j.envint.2020.105814>, 2020b.
- Ramanathan, V., Crutzen, P. J., Lelieveld, J., Mitra, A. P., Althausen, D., Anderson, J., Andreae, M. O., Cantrell, W., Cass, G. R., Chung, C. E., Clarke, A. D., Coakley, J. A., Collins, W. D., Conant, W. C., Dulac, F., Heintzenberg, J., Heysfield, A. J., Holben, B., Howell, S., Hudson, J., Jayaraman, A., Kiehl, J. T., Krishnamurti, T. N., Lubin, D., McFarquhar, G., Novakov, T., Ogren, J. A., Podgorny, I. A., Prather, K., Priestley, K., Prospero, J. M., Quinn, P. K., Rajeev, K., Rasch, P., Rupert, S., Sadourny, R., Satheesh, S. K., Shaw, G. E., Sheridan, P. and Valero, F. P. J.: Indian Ocean Experiment: An integrated analysis of the climate forcing and effects of the great Indo-Asian haze, *J. Geophys. Res.-Atmos.*, 106, 28371–28398, <https://doi.org/10.1029/2001JD900133>, 2001.
- Ramanathan, V., Chung, C., Kim, D., Bettge, T., Buja, L., Kiehl, J. T., Washington, W. M., Fu, Q., Sikka, D. R., and Wild, M.: Atmospheric brown clouds: Impacts on South Asian climate and hydrological cycle, *P. Natl. Acad. Sci. USA*, 102, 5326–5333, <https://doi.org/10.1073/pnas.0500656102>, 2005.
- Robrecht, S., Vogel, B., Grooß, J.-U., Rosenlof, K., Thornberry, T., Rollins, A., Krämer, M., Christensen, L., and Müller, R.: Mechanism of ozone loss under enhanced water vapour conditions in the mid-latitude lower stratosphere in summer, *Atmos. Chem. Phys.*, 19, 5805–5833, <https://doi.org/10.5194/acp-19-5805-2019>, 2019.
- Romatschke, U. and Houze, R. A.: Characteristics of precipitating convective systems in the South Asian monsoon, *J. Hydrometeorol.*, 12, 3–26, <https://doi.org/10.1175/2010JHM1289.1>, 2011.
- Satheesh, S. K. and Ramanathan, V.: Large differences in tropical aerosol forcing at the top of the atmosphere and Earth's surface, *Nature*, 405, 60–63, <https://doi.org/10.1038/35011039>, 2000.
- Satheesh, S. K., Ramanathan, V., Holben, B. N., Krishna Moorthy, K., Loeb, N. G., Mating, H., Prospero, J. M., and Savoie, D.: Chemical, microphysical, and radiative effects of Indian Ocean aerosols, *J. Geophys. Res.*, 107, 4725, <https://doi.org/10.1029/2002JD002463>, 2002.
- Shindell, D. T.: Climate and ozone response to increased stratospheric water vapor, *Geophys. Res. Lett.*, 28, 1551–1554, <https://doi.org/10.1029/1999GL011197>, 2001.
- Shindell, D. T., Chin, M., Dentener, F., Doherty, R. M., Faluvegi, G., Fiore, A. M., Hess, P., Koch, D. M., MacKenzie, I. A., Sanderson, M. G., Schultz, M. G., Schulz, M., Stevenson, D. S., Teich, H., Textor, C., Wild, O., Bergmann, D. J., Bey, I., Bian, H., Cuvelier, C., Duncan, B. N., Folberth, G., Horowitz, L. W., Jonson, J., Kaminski, J. W., Marmer, E., Park, R., Pringle, K. J., Schroeder, S., Szopa, S., Takemura, T., Zeng, G., Keating, T. J., and Zuber, A.: A multi-model assessment of pollution transport to the Arctic, *Atmos. Chem. Phys.*, 8, 5353–5372, <https://doi.org/10.5194/acp-8-5353-2008>, 2008.
- Stier, P., Feichter, J., Kinne, S., Kloster, S., Vignati, E., Wilson, J., Ganzeveld, L., Tegen, I., Werner, M., Balkanski, Y., Schulz, M., Boucher, O., Minikin, A., and Petzold, A.: The aerosol-climate model ECHAM5-HAM, *Atmos. Chem. Phys.*, 5, 1125–1156, <https://doi.org/10.5194/acp-5-1125-2005>, 2005.

- Solomon, S., Rosenlof, K. H., Portmann, R. W., Daniel, J. S., Davis, S. M., Sanford, T. J., and Plattner, G. K.: Contributions of stratospheric water vapor to decadal changes in the rate of global warming, *Science*, 327, 1219–1223, <https://doi.org/10.1126/science.1182488>, 2010.
- Taylor, K. E., Williamson, D. L., and Zwiers, F. W.: The Sea Surface Temperature and Sea-Ice Concentration Boundary Conditions for AMIP II Simulations, Program for Climate Model Diagnosis and Intercomparison (PCMDI), Lawrence Livermore Natl. Lab. Livermore, Calif. Rep., 60, 1–28, 2000.
- Tegen, I., Harrison, S. P., Kohfeld, K. E., Prentice, I. C., Coe, M., and Heimann, M.: Impact of vegetation and preferential source areas on global dust aerosol: Results from a model study, *J. Geophys. Res.-Atmos.*, 107, 14–27, <https://doi.org/10.1029/2001JD000963>, 2002.
- Tegen, I., Neubauer, D., Ferrachat, S., Siegenthaler-Le Drian, C., Bey, I., Schutgens, N., Stier, P., Watson-Parris, D., Stanelle, T., Schmidt, H., Rast, S., Kokkola, H., Schultz, M., Schroeder, S., Daskalakis, N., Barthel, S., Heinold, B., and Lohmann, U.: The global aerosol–climate model ECHAM6.3–HAM2.3 – Part 1: Aerosol evaluation, *Geosci. Model Dev.*, 12, 1643–1677, <https://doi.org/10.5194/gmd-12-1643-2019>, 2019.
- Waugh, D. W. and Polvani, L. M.: Intrusions into the tropical upper troposphere, *Geophys. Res. Lett.*, 27, 3857–3860, <https://doi.org/10.1029/2000GL012250>, 2000.
- Yan, X., Konopka, P., Hauck, M., Podglajen, A., and Ploeger, F.: Asymmetry and pathways of inter-hemispheric transport in the upper troposphere and lower stratosphere, *Atmos. Chem. Phys.*, 21, 6627–6645, <https://doi.org/10.5194/acp-21-6627-2021>, 2021.
- Yue, J., Russell, J., Gan, Q., Wang, T., Rong, P., Garcia, R., and Mlynczak, M.: Increasing Water Vapor in the Stratosphere and Mesosphere After 2002, *Geophys. Res. Lett.*, 46, 13452–13460, <https://doi.org/10.1029/2019GL084973>, 2019.
- Zhang, K., O'Donnell, D., Kazil, J., Stier, P., Kinne, S., Lohmann, U., Ferrachat, S., Croft, B., Quaas, J., Wan, H., Rast, S., and Feichter, J.: The global aerosol-climate model ECHAM-HAM, version 2: sensitivity to improvements in process representations, *Atmos. Chem. Phys.*, 12, 8911–8949, <https://doi.org/10.5194/acp-12-8911-2012>, 2012.
- Zheng, C., Wu, Y., Ting, M., Orbe, C., Wang, X., and Tilmes, S.: Summertime transport pathways from different northern hemisphere regions into the Arctic, *J. Geophys. Res.-Atmos.*, 126, e2020JD033811, <https://doi.org/10.1029/2020JD033811>, 2021.